Impact of stresses and alloying elements on ferrous martensite nanodomains

Paul Eyméoud, Dmytro Kandaskalov, Philippe Maugis

Graphical Abstract

Impact of Ni alloying on Fe-C martensite ageing: an atomistic investigation

Paul Eyméoud,Liangzhao Huang,Philippe Maugis

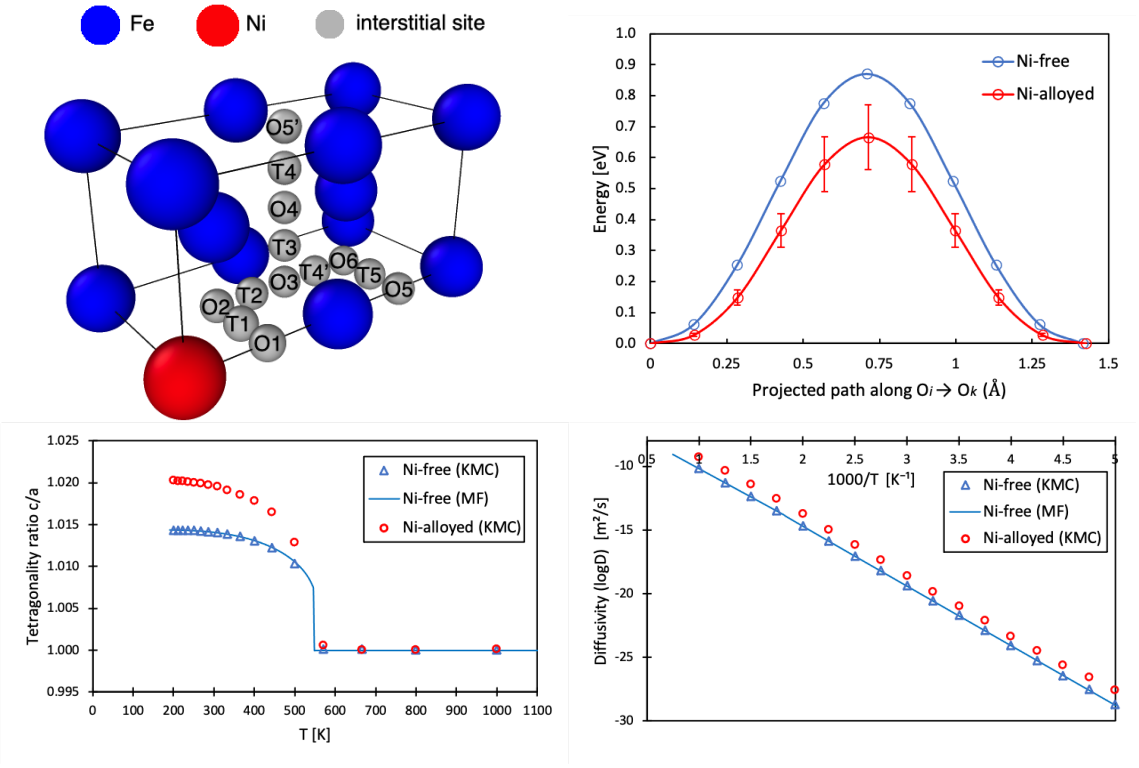

Highlights

Impact of Ni alloying on Fe-C martensite ageing: an atomistic investigation

Paul Eyméoud,Liangzhao Huang,Philippe Maugis

- Computational investigation combining first-principles and Kinetic Monte-Carlo approaches.
- Ni alloying lowers migration energies and force dipole tensor components associated to an interstitial C in α-Fe.
- Ni alloying accelerates ageing kinetics.

Impact of Ni alloying on Fe-C martensite ageing: an atomistic investigation

Paul Eyméoud[a,*], Liangzhao Huang[a] and Philippe Maugis[a]

[a]Aix-Marseille Univ, CNRS, IM2NP Marseille, France

ARTICLE INFO

Keywords:
Martensite ageing
Fe-Ni-C
Carbon diffusion
Climbing Image Nudged Elastic Band
Kinetic Monte-Carlo
Mean-field elastic model

ABSTRACT

We propose a computational investigation of Ni-alloying impact on Fe-C martensite ageing, at the atomic scale. Using the Climbing Image Nudged Elastic Band technique, we showed the repulsive nature of Ni-C pairwise interactions in α-iron, and demonstrated that Ni alloying lowers the migration energies and force dipole tensor components associated to an interstitial carbon in α-iron. Computed values of pairwise interactions, migration energies and dipole components were used to implement a Kinetic Monte-Carlo approach. We found that Ni alloying: *(i)* has negligible impact on martensite thermodynamical stability, *(ii)* accelerates ageing kinetics, by increasing carbon diffusivity.

Thermal ageing induces important changes on ferrous martensite properties [1], such as hardness [2, 3, 4], strength [5, 6], and thermal expansion [7, 8]. Numerous experimental and theoretical works carried out to understand these changes revealed that carbon redistribution on octahedral interstitial sublattices (o.i.s.) is one of the major driving forces of the ageing process [9, 10, 11, 12, 13, 14].

This carbon redistribution during martensite ageing can be biased by several factors, not only applied stresses [10, 15], grain structure [16] and crystal defects [17], but also alloying elements. In this sense, the case of Ni-alloying is of particular interest, notably for maraging steels conception [18]. Although numerous ageing studies were performed on both non-alloyed [19, 20] and Ni-alloyed martensite [13, 21, 22, 23], few studies have compared the two cases, except as concerns tetragonality changes [24, 25, 16, 26]. By compiling those experimental data on martensite ageing, it appears difficult to separate what depends or not on Ni alloying.

To shed light on the matter, the present work aims at evaluating the impact of Ni alloying on martensite ageing, by combining first-principles and Kinetic Monte-Carlo (KMC) computational approaches. Although close computational investigations have been already performed for other alloying cases, such as Fe-Si-C [27], Fe-Cr-C [28] or Fe-Nb-C [29], the project appears as new for Fe-Ni-C system.

The study falls into two parts. First, we realized a bipartite first-principles study of the impact of Ni addition on interstitial carbon dipole tensors and migration energies: in the dilute limit, and for 25at%Ni alloying. Second, using the previously computed first-principles data, we implemented a KMC procedure, validated it on Mean-Field (MF) calculations, and used it to study the impact of Ni alloying on martensite(α')-ferrite(α) transition and carbon diffusivity.

First-principles calculations have been performed with VASP code [30, 31], with generalized gradient approximation [32] with projector augmented wave method [33] and Perdew-Burke-Ernzerhof exchange-correlation functionals [34, 35], spin polarized approximation, 400 eV energy cut-off, $4\times4\times4$ Monkhorst-Pack scheme [36] for k-points meshes construction, 10^{-5} eV energy convergence criterion for electronic self-consistency. As concerns ionic relaxations, RMM-DIS algorithm [37] was used with $0.001\text{eV}/\text{Å}^3$ ionic relaxation criterion, except for $Fe_{96}Ni_{32}C_1$ supercells ($0.0075\text{eV}/\text{Å}^3$). To reproduce carbon migration paths, Climbing Image Nudged Elastic Band (CI-NEB) methodology has been used for fixed lattice volume and geometry (only internal relaxations were allowed), with 9 intermediary images, and $0.05\text{eV}/\text{Å}^3$ ionic relaxation criterion. To simulate 25at%Ni alloying (Fe-Ni disorder on host sublattice), we have built a $Fe_{96}Ni_{32}$ Special Quasirandom Structure [38] (SQS), using the *mcsqs* module [39] of ATAT code [40]: calculation of the correlation functions has been performed on clusters containing atomic pairs shorter or equal to $\sqrt{3}a_0$. Additional information on DFT numerical implementation and results are given in Supplementary Material (SM).

In order to understand the impact of Ni on carbon migration, we started with the influence of dilute Ni alloying on interstitial carbon. First of all, we determined the neighboring concentric shells of octahedral and tetrahedral sites surrounding a substitutional Ni (cf. Fig. 1, top left). For each possible carbon position, the Ni-C pairwise interaction energy is defined as [41]:

$$\begin{aligned} V(\text{Ni}-\text{C}) \quad = \quad & E(\text{Fe}_{127}\text{Ni}_1\text{C}_1) + E(\text{Fe}_{128}) \\ & - E(\text{Fe}_{127}\text{Ni}_1) - E(\text{Fe}_{128}\text{C}_1) \end{aligned}$$

wherein all supercells are taken at the fixed lattice volume and shape of the $Fe_{127}Ni_1$ equilibrium one. Such formulation enables the calculation of elastic dipoles associated with C atoms (relaxation due to C ordering will be integrated later, in the thermostatistical study). For the octahedral (resp. tetrahedral) cases, $Fe_{128}C_1$ and $Fe_{127}Ni_1C_1$ supercells were computed by performing internal relaxations (resp. CI-NEB procedure). The results, presented in Fig. 1, top center, reveal that : *(i)* Ni-C octahedral-type pairs are strongly repulsive up to second neighbors and negligible be-

*Corresponding author.
paul.eymeoud@univ-amu.fr (P. Eyméoud)
ORCID(s): 0000-0003-4705-4244 (P. Eyméoud); 0000-0001-8483-4560 (L. Huang); 0000-0001-9283-0471 (P. Maugis)

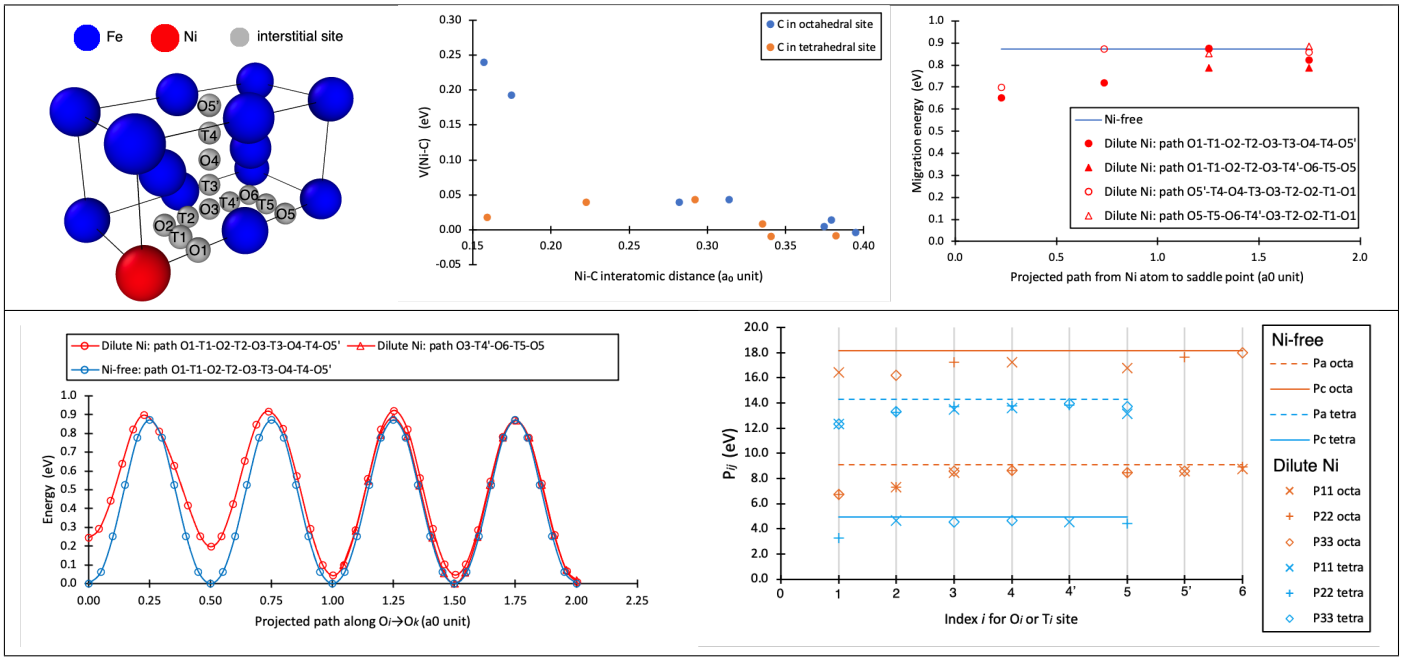

Figure 1: Top left: neighboring shells of octahedral and tetrahedral interstitial sites surrounding a substitutional Ni atom. Top center: associated values for V(Ni-C) pairwise interaction, with Ni-C interatomic distance after internal relaxations. Bottom left : energetic profiles of carbon migration along the $O_i \longrightarrow T_j \longrightarrow O_k$ paths (energy reference: carbon on O6). Top right: associated migration energies. Bottom right: associated dipole components for C located on tetrahedral and octahedral sites.

yond, *(ii)* Ni-C tetrahedral-type pairs are negligible (particularly, T_1 pair is widely less repulsive than O_1 and O_2 ones).

In a second part, we have computed by CI-NEB approach the migration energy profile associated to each tetrahedral site and its two nearest octahedral neighboring sites. The results, presented on Fig. 1, bottom left and top right, reveal that Ni reduces migration energy E_0^m (*i.e.*, energy difference between saddle point energy and initial stable state energy) by about 20% for the first and second neighboring shells (paths $O_1 \longrightarrow T_1 \longrightarrow O_2$ and $O_2 \longrightarrow T_2 \longrightarrow O_3$), and this effect vanishes for higher order neighboring. Associated force dipole tensor components, presented in Fig. 1, bottom right, reveal the strong impact of Ni for O_1, O_2 and T_1 (reduction by 20%) and less important impact beyond.

In order to evaluate the effect of 25at%Ni alloying on C migration, we have applied the CI-NEB methodology to construct the $O-T-O$ migration paths related to ten tetrahedral sites randomly chosen in the $Fe_{96}Ni_{32}$ SQS. After averaging the paths (arithmetical average on SQS, see Ref. [15]), in both back and forth directions of migration (see Ref. [42, 27]), we got the migration energy and force dipole tensor components presented in Fig. 2. It gives a rough estimate of Ni-induced lowering, by combining both strong E_0^m lowering induced by O_1, O_2 configurations, and weaker E_0^m lowering induced by higher order neighboring shells (O_3, O_4, *etc.*). This procedure reveals that 25at%Ni alloying lowers migration energy (resp. force dipole tensor components) by about 25% (resp. 40%).

Moreover, the Ni-induced lowering of migration energy and dipole components are coherent with experimental data

	0at%Ni	25at%Ni
a_0 (Å), C-free lattice	2.831	2.851
C_{11} (GPa), C-free lattice	282.7	189.5
C_{12} (GPa), C-free lattice	148.7	119.1
C_{44} (GPa), C-free lattice	99.7	114.4
P_a (eV), C in o.i.s.	9.1	4.9
P_c (eV), C in o.i.s.	18.2	11.8
P_a (eV), C in t.i.s.	14.3	9.8
P_c (eV), C in t.i.s.	5.0	2.75
E_0^m (eV)	0.871	0.665

Table 1
Parameters computed in the framework of DFT. Elastic constants have been computed using the VASP parameterization from [46] on a two-iron atoms body-centered cubic unit cell for Ni-free case, and our usual VASP parameterization on a $Fe_{12}Ni_4$ SQS supercell for Ni-alloyed case.

plotted on Fig. 2. Experimental values of dipole components for C atom in octahedral sites have been computed using formulas (7,8) from Ref. [26], wherein δ_a and δ_c values have been extracted from X-ray diffraction data of [43] (resp. [44, 45]) for Ni-free (resp. Ni-alloyed) case.

In order to evaluate the impact of Ni-alloying on martensite ageing, we used the parameters resulting from our DFT investigation, to implement a KMC approach.

In this KMC approach, we applied the residence-time algorithm on 2×32^3 bcc sites simulation box with periodic boundary conditions. 25at% Ni-alloying was reproduced by a random distribution of Ni on host lattice. About 1000 C atoms were inserted in the simulation box (corresponding to

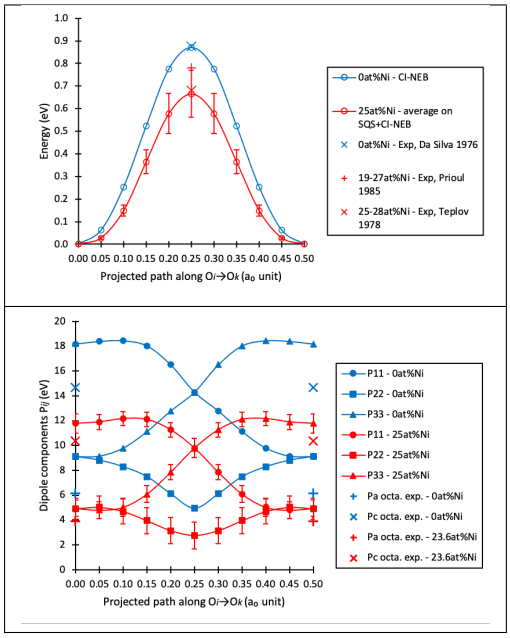

Figure 2: Migration energy profile versus reaction coordinate (top), and associated variation of dipole components (bottom): blue (resp. red) for Ni-free (resp. Ni-alloyed) case. Experimental data extracted from [47, 48, 49, 43, 44, 45].

1.5at% of C), and allowed to jump during the simulation. For jump frequencies, we employed the following expression:

$$\Gamma_{ij} = \nu_0 \exp\big(-(E_0^m - (\mathbf{P}^{\mathrm{T_j}} - \mathbf{P}^{\mathrm{O_i}}) : \boldsymbol{\varepsilon})/(\mathrm{k_B T})\big) \quad (1)$$

where $\boldsymbol{\varepsilon}$ denotes the homogeneous strain tensor induced by the carbon atoms on octahedral positions (pure dilatation in ferrite, tetragonal distortion in martensite), $\mathbf{P}^{\mathrm{T_j}}$ (resp. $\mathbf{P}^{\mathrm{O_i}}$) the dipole tensor associated to carbon atom (considered as independent of the chemical environment) in t.i.s. (resp. o.i.s.), E_0^m the migration energy of undeformed crystal, and ν_0 the attempt frequency. This last one is assumed to be: *(i)* strain-independent, *(ii)* the same in Ni-free and Ni-alloyed cases, since alloying-induced elastic modulus variations (about 20-30%) generates minor variations of ν_0 (about 10-20%) [50, 51]. In the Ni-alloyed case, the quantity E_0^m is given by the pairwise approximation:

$$\begin{aligned} E_0^m(\text{Ni-alloyed}) &= E_0^m(\text{Ni-free}) + \sum_{i \in \text{ neighboring T sites}} z_i V^i_{\text{Ni-C}} \\ &\quad - \sum_{i \in \text{ neighboring O sites}} z_i V^i_{\text{Ni-C}} \end{aligned} \quad (2)$$

where z_i denotes the number of Ni atoms at the shell i of the considered C atom, E_0^m(Ni-free) is contained in first column of Table 1, and $V^i_{\text{Ni-C}}$ are plotted on Fig. 1, top center. Such technique allows us to take into account the local Ni environment of C, instead of working with the approximated migration energy of Table 1, column 2, obtained by averaging.

To estimate the Zener order parameter, carbon interstitial occupancies were measured after each atomic jump (associated lattice parameters were then deduced from Eq. (4,5)). After the system reached equilibrium, 100 measurements of the mean squared displacement (MSD) of carbon atoms after 3×10^5 atomic jumps (*i.e.*, a total of 3×10^7 carbon jumps for each simulation) were performed to compute the tracer diffusion coefficients. The relative convergence of the obtained C diffusivities was taken within $\pm1\%$ with these settings.

Tracer diffusivity D_i $(i = x, y, z)$ is related to the MSD $\langle R_i^2 \rangle$ along the x, y, z directions during a period of time τ via the Einstein-Smoluchowski equation $\langle R_i^2 \rangle = 2D_i\tau$. The MSD is given by:

$$\langle R_i^2 \rangle = \left\langle \left(\sum_{n=1}^{N} R_{n,i} \right)^2 \right\rangle = f_i \left\langle \left(\sum_{n=1}^{N} R_{n,i}^2 \right) \right\rangle \quad (3)$$

where N is the total number of jumps in the period of time τ and $R_{n,i}$ is the displacement of a C atom along the i-direction due to the n-th jumps. $\langle (\sum_{n=1}^{N} R_{n,i}^2) \rangle$ is the uncorrelated MSD corresponding to the random diffusion path, and f_i is the correlation factor characterising deviation between the tracer diffusion and a random walk.

From the thermodynamical point of view, our KMC approach allowed us to deduce the thermal evolution of Zener order parameter $\eta = (c_1 - (c_2 + c_3)/2)/C$ (where c_1, c_2, c_3, respectively denotes carbon fraction on x, y, z oriented o.i.s., and $C = c_1 + c_2 + c_3$) to describe ordering transition between martensite α' ($\eta \approx 1$: C atoms preferentially located on z – o.i.s.) and ferrite α ($\eta = 0$: C atoms evenly distributed on the three o.i.s.). Associated variations of lattice parameters, presented on Fig. 3, top left were then inferred from [53]:

$$a/a_0 = 1 + 2C\big[\kappa - \theta \cdot \eta\big]/(3a_0^3) \quad (4)$$

$$c/a_0 = 1 + 2C\big[\kappa + 2\theta \cdot \eta\big]/(3a_0^3) \quad (5)$$

with $\kappa = (S_{11}+2S_{12})(P_c+2P_a)$ and $\theta = (S_{11}-S_{12})(P_c-P_a)$, where S_{11}, S_{12} (resp. P_c, P_a) denote the compliance (resp. dipole) tensor components. Formula (4,5) were also used to compute the ε strain tensor appearing in Eq. (1).

From the kinetical point of view, our KMC approach led to the Arrhenius plots of total diffusivity $D = D_x + D_y + D_z$ presented on Fig. 3, top right.

Before analyzing our KMC results, we have first validated the KMC model in the Ni-free case, by comparing it to the calculations performed using Maugis's mean-field elastochemical model [53, 54], implemented with the parameters from left column of Table 1.

This MF model starts from the following expression of the elastic part of the energy of the crystal (per iron atom) containing a population of point defects (namely, interstitial carbon atoms), submitted to an homogeneous strain $\boldsymbol{\varepsilon}$ relative to carbon-free lattice [53]:

$$E^{el} = a_0^3\big[\mathbf{C}\boldsymbol{\varepsilon} : \boldsymbol{\varepsilon} - \mathcal{P} : \boldsymbol{\varepsilon}\big]/4 \quad (6)$$

wherein $\mathbf{C}$, $\mathcal{P}$, $\boldsymbol{\varepsilon}$ respectively denotes stiffness, volume density of force dipole, and homogeneous strain tensor, and a_0 is the equilibrium lattice parameter of carbon-free lattice. In this framework, under zero-stress, equation (6) leads to the energy at mechanical equilibrium $E^{el} = -h_\Sigma C^2 \eta^2$ wherein $h_\Sigma = 2(S_{11} - S_{12})(P_c - P_a)^2/(3a_0^3)$ is the strain-energy parameter. It then can be shown that the α'-α equilibrium Zener

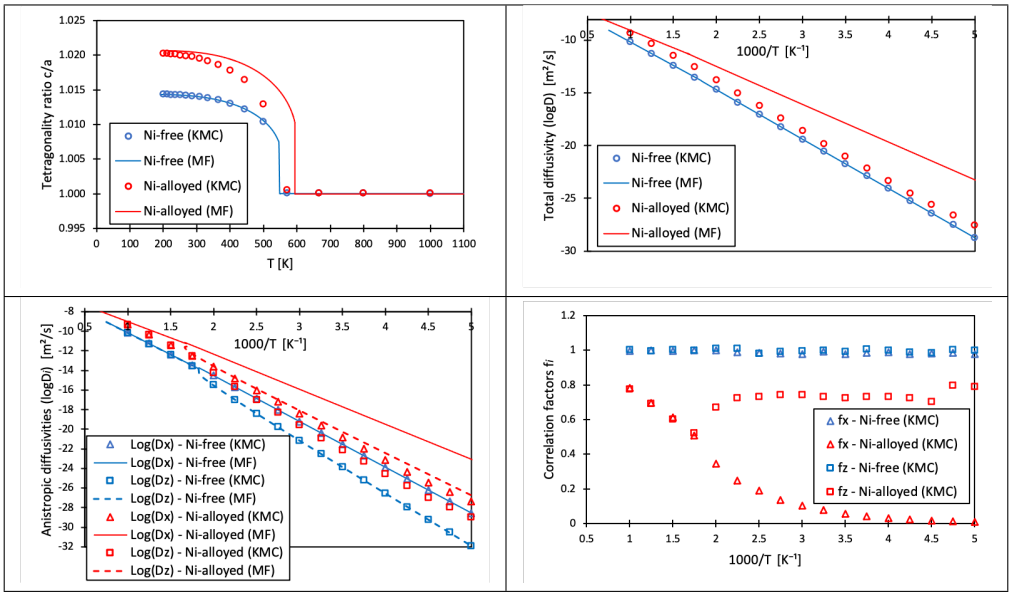

Figure 3: Effects of 25at%-Ni-alloying on: *(i)* thermodynamics: evolution of tetragonality ratio c/a with temperature (top left), *(ii)* kinetics: Arrhenius plots of total diffusivity (top right), anisotropic diffusivities (bottom left), correlation factors (bottom right). Calculations performed in MF and KMC, using $C = 1.5\text{at}\%$ and $\nu_0 = 149\text{THz}$ [52].

order parameter η at temperature T is governed by the implicit equation (see Eq. (18) from Ref. [53]):

$$3Ch_\Sigma\eta + k_B T \ln\big((1+2\eta)/(1-\eta)\big) = 0 \tag{7}$$

By solving Eq. (7), one can then infer the lattice parameters through Eq. (4, 5). Concerning the kinetical aspects, the MF anisotropic diffusivities are deduced using Eq. (1), and the following equations [52] (c, a deduced from Eq. (4,5)):

$$D_x = D_y = \frac{a^2}{2}\frac{\Gamma_{31}\Gamma_{12}}{2\Gamma_{31}+\Gamma_{12}}, \quad D_z = \frac{c^2}{2}\frac{\Gamma_{31}\Gamma_{13}}{2\Gamma_{31}+\Gamma_{12}} \tag{8}$$

Comparing our KMC and MF results in Ni-free case, we got the superimposed blue plots in Fig. 3 top left, top right and bottom left, which validates our KMC procedure.

After this validation, we have compared our KMC results in Ni-free and Ni-alloyed case.

From the thermodynamical point of view, considering Fig. 3, top left we conclude that Ni-alloying: *(i)* has negligible impact on α'-α transition temperature, *(ii)* increases the tetragonality ratio at low temperature. This second point, coherent with experimental data from [16, 24], is linked to the Ni-induced host lattice softening, noticeable on C_{ij} values from Table 1 (see Ref. [26] for detailed justification).

From the kinetical point of view, considering the Arrhenius plots of total diffusivity in Fig. 3, top right (resulting from the anisotropic diffusivities from Fig. 3, bottom left), we conclude that Ni-alloying increases carbon diffusivity: by a factor 5.7 at 300K (α' domain), and a factor 8.7 at 700K (α domain). Such particular behavior contrasts with C diffusivity decreasing modeled in Fe-Cr [28] or Fe-Si [27] alloys. What is more, we can notice on Fig. 3, bottom right the strong changes on correlation factors induced by Ni-alloying, particularly in α' domain. Those correlation factors slightly differs from 1 in non-alloyed case, since a C atom is not allowed to jump on a site which is already occupied by another C atom. We also realized a comparative approximated Ni-alloyed MF modeling (red curves on Fig. 3): it is not quantitatively valid, since it does not take into account neither local chemistry, nor kinetic correlations.

To conclude, we have shown by first-principles calculations that: *(i)* Ni-C pairwise interactions are strongly repulsive up to second neighboring, *(ii)* Ni-alloying lowers migration energy and force dipole tensor components associated to interstitial carbon in ferrite and martensite. Implementing numerical values of those energetic parameters in a KMC procedure (validated on MF calculations in Ni-free case), allowed us to see the Ni-alloying impact on martensite ageing. Thermodynamically, Ni-alloying has negligible impact on martensite stability, since α'-α transition temperature remains quite unchanged. Kinetically, Ni-alloying accelerates ageing kinetics, by increasing carbon diffusivity.

Acknowledgments, Data availability statement

This work was supported by the Agence Nationale de la Recherche (contract C-TRAM ANR-18-CE92-0021). Centre de Calcul Intensif d'Aix-Marseille is acknowledged for granting access to its high performance computing resources. P. Eyméoud thanks D. Kandaskalov for providing useful numerical tools to implement NEB for Fe-C system.

Data are available upon request.

References

[1] K. A. Taylor and M. Cohen *Progress in Materials Science*, vol. 36, p. 225, 1992. https://doi.org/10.1016/0079-6425(92)90010-5.

[2] P. G. Winchell and M. Cohen *Transactions ASM*, vol. 55, p. 347, 1962.

[3] G. Krauss *Materials Science and Engineering*, vol. A273-275, p. 40, 1999. https://doi.org/10.1016/S0921-5093(99)00288-9.

[4] S. E. Hartfield. Master thesis, MIT, 1988. https://dspace.mit.edu/bitstream/handle/1721.1/27960/18463434-MIT.pdf?sequence=2.

[5] G. T. Eldis and M. Cohen *Metallurgical Transactions A*, vol. 14A, p. 1007, 1983. https://doi.org/10.1007/BF02659848.

[6] M. Calcagnotto, Y. Adachi, D. Ponge, and D. Raabe *Acta Materialia*, vol. 59, p. 658, 2011. https://doi.org/10.1016/j.actamat.2010.10.002.

[7] V. H. Gerdien *Archiv für das Eisenhüttenwesen*, vol. 11, p. 673, 1959. https://doi.org/10.1002/srin.195903098.

[8] L. Cheng, C. M. Brakman, B. M. Korevaar, and E. J. Mittemeijer *Metallurgical Transactions A*, vol. 19A, p. 2415, 1988. https://doi.org/10.1007/BF02645469.

[9] G. V. Kurdjumov *Metallurgical Transactions A*, vol. 7A, p. 999, 1976. https://doi.org/10.1007/BF02644066.

[10] P. Maugis *Journal of Phase Equilibria and Diffusion*, vol. 41, p. 269, 2020. https://doi.org/10.1007/s11669-020-00816-2.

[11] G. V. Kurdjumov and A. G. Khachaturyan *Acta Metallurgica*, vol. 23, p. 1077, 1975. https://doi.org/10.1016/0001-6160(75)90112-1.

[12] S. Allain, F. Danoix, M. Goune, K. Hoummada, and D. Mangelinck *Philosophical Magazine Letters*, vol. 93, p. 68, 2013. https://doi.org/10.1080/09500839.2012.742590.

[13] P. C. Chen and P. G. Winchell *Metallurgical Transactions A*, vol. 11A, p. 1333, 1980. https://doi.org/10.1007/BF02653487.

[14] R. Kaplow, M. Ron, and N. DeCristofaro *Metallurgical Transactions A*, vol. 14A, p. 1135, 1983. https://doi.org/10.1007/BF02670451.

[15] P. Maugis, D. Connétable, and P. Eyméoud *Scripta Materialia*, vol. 194, p. 113632, 2021. https://doi.org/10.1016/j.scriptamat.2020.113632.

[16] S. Kajiwara and T. Kikuchi *Acta Metallurgica et Materialia*, vol. 39,6, p. 1123, 1991. https://doi.org/10.1016/0956-7151(91)90200-K.

[17] B. Lüthi, F. Berthier, L. Ventelon, B. Legrand, D. Rodney, and F. Willaime *Modelling and Simulation in Materials Science and Engineering*, vol. 27, p. 074002, 2019. https://doi.org/10.1088/1361-651X/ab28d4.

[18] A. P. Mouritz, *Introduction to aerospace materials*. Elsevier, 2012.

[19] L. Cheng, N. M. V. der Pers, A. Böttger, T. H. de Keijser, and E. J. Mittemeijer *Metallurgical Transactions A*, vol. 22 A, p. 1957, 1991. https://doi.org/10.1007/BF02669863.

[20] W. K. Choo and R. Kaplow *Acta Metallurgica*, vol. 21, p. 725, 1973. https://doi.org/10.1016/0001-6160(73)90036-9.

[21] K. A. Taylor, L. Chang, G. B. Olson, G. D. W. Smith, M. Cohen, and J. B. V. Sande *Metallurgical Transactions A*, vol. 20A, p. 2717, 1989. https://doi.org/10.1007/BF02670166.

[22] A. M. Sherman, G. T. Eldis, and M. Cohen *Metallurgical Transactions A*, vol. 14A, p. 995, 1983. https://doi.org/10.1007/BF02659847.

[23] M. K. Miller, P. A. Beaven, S. S. Brenner, and G. D. W. Smith *Metallurgical Transactions A*, vol. 14A, p. 1021, 1983. https://doi.org/10.1007/BF02670440.

[24] G. V. Kurdjumov, L. K. Mikhailova, and A. G. Khachaturyan *Doklady Akademii Nauk USSR*, vol. 215, p. 578, 1974. https://www.researchgate.net/publication/253288965_Anomalously_high_tetragonality_of_martensite_with_high_nickel_content_and_the_nature_of_the_anomalies_of_the_tetragonality.

[25] P. G. Winchell. Doctoral dissertation, MIT, 1958. https://dspace.mit.edu/handle/1721.1/51540.

[26] S. Chentouf, S. Cazottes, F. Danoix, M. Goune, H. Zapolsky, and P. Maugis *Intermetallics*, vol. 89, p. 92, 2017. https://doi.org/10.1016/j.intermet.2017.05.022.

[27] D. Simonovic, C. K. Ande, A. I. Duff, F. Syahputra, and M. H. F. Sluiter *Physical Review B*, vol. 81, p. 054116, 2010. https://doi.org/10.1103/PhysRevB.81.054116.

[28] R. Herschberg, C.-C. Fu, M. Nastar, and F. Soisson *Acta Materialia*, vol. 165, p. 638, 2019. https://doi.org/10.1016/j.actamat.2018.11.025.

[29] D. Gendt, P. Maugis, G. Martin, M. Nastar, and F. Soisson *Defect and Diffusion Forum*, vol. 194-199, p. 1779, 2001. https://doi.org/10.4028/www.scientific.net/DDF.194-199.1779.

[30] G. Kresse and J. Furthmüller *Computational Materials Science*, vol. 6, p. 15, 1996. https://doi.org/10.1016/0927-0256(96)00008-0.

[31] G. Kresse and J. Furthmüller *Physical Review B*, vol. 54, p. 11169, 1996. https://doi.org/10.1103/PhysRevB.54.11169.

[32] G. Kresse and D. Joubert *Physical Review B*, vol. 59, p. 1758, 1999. https://doi.org/10.1103/PhysRevB.59.1758.

[33] P. E. Blöchl *Physical Review B*, vol. 50, p. 17953, 1994. https://doi.org/10.1103/PhysRevB.50.17953.

[34] J. P. Perdew, K. Burke, and M. Ernzerhof *Physical Review Letters*, vol. 77, p. 3865, 1996. https://doi.org/10.1103/PhysRevLett.77.3865.

[35] J. P. Perdew, K. Burke, and M. Ernzerhof *Physical Review Letters*, vol. 78, p. 1396, 1997. https://doi.org/10.1103/PhysRevLett.78.1396.

[36] H. J. Monkhorst and J. D. Pack *Physical Review B*, vol. 13, p. 5188, 1976. https://doi.org/10.1103/PhysRevB.13.5188.

[37] P. Pulay *Chemical Physics Letters*, vol. 73, p. 393, 1980. https://doi.org/10.1016/0009-2614(80)80396-4.

[38] A. Zunger, S. H. Wei, L. G. Ferreira, and J. E. Bernard *Physical Review Letters*, vol. 65, p. 353, 1990. https://doi.org/10.1103/PhysRevLett.65.353.

[39] A. Van de Walle, P. Tiwary, M. De Jong, D. L. Olmsted, M. Asta, A. Dick, D. Shin, Y. Wang, L. Q. Chen, and Z. K. Liu *Calphad*, vol. 42, p. 13, 2013. https://doi.org/10.1016/j.calphad.2013.06.006.

[40] A. Van de Walle, M. Asta, and G. Ceder *Calphad*, vol. 26, p. 539, 2002. https://doi.org/10.1016/S0364-5916(02)80006-2.

[41] A. A. Mirzoev, Y. M. Ridnyi, and A. V. Verkhovykh *Russian Metallurgy (Metally)*, vol. 2019, p. 168, 2019. https://doi.org/10.1134/S0036029519020174.

[42] A. Van der Ven, G. Ceder, M. Asta, and P. D. Tepesch *Physical Review B*, vol. 64, p. 184307, 2001. https://doi.org/10.1103/PhysRevB.64.184307.

[43] L. Cheng, A. Böttger, T. H. de Keijser, and E. J. Mittemeijer *Scripta Metallurgica et Materialia*, vol. 24, p. 509, 1990. https://doi.org/10.1016/0956-716X(90)90192-J.

[44] L. Zwell, D. E. Carnahan, and G. R. Speich *Metallurgical Transactions*, vol. 1, p. 1007, 1970. https://doi.org/10.1007/BF02811785.

[45] L. Lyssak, V. E. Danilchenko, and V. A. Okhrimenko *Scripta Metallurgica*, vol. 16, p. 649, 1982. https://doi.org/10.1016/0036-9748(82)90315-5.

[46] M. R. Fellinger, L. G. H. Jr, and D. R. Trinkle *Computational Materials Science*, vol. 126, p. 503, 2017. https://doi.org/10.1016/j.commatsci.2016.09.040.

[47] J. R. G. D. Silva and R. B. McLellan *Materials Science and Engineering*, vol. 26, p. 83, 1976. https://doi.org/10.1016/0025-5416(76)90229-9.

[48] C. Prioul *Journal de Physique Colloques*, vol. 46 C10, pp. C10–665, 1985. https://doi.org/10.1051/jphyscol:198510147.

[49] V. A. Teplov *The Physics of Metals and Metallography*, vol. 46(1), p. 141, 1978.

[50] C. Kittel, *Introduction to Solid State Physics, 8th Edition*. John Wiley & Sons, Inc., 2004.

[51] D. Kandaskalov and P. Maugis *Computational Materials Science*, vol. 128, p. 278, 2017. https://doi.org/10.1016/j.commatsci.2016.11.022.

[52] P. Maugis, S. Chentouf, and D. Connétable *Journal of Alloys and Compounds*, vol. 769, p. 1121, 2018. https://doi.org/10.1016/j.jallcom.2018.08.060.

[53] P. Maugis *Acta Materialia*, vol. 158, p. 454, 2018. https://doi.org/10.1016/j.actamat.2018.08.001.

[54] P. Maugis *Computational Materials Science*, vol. 159, p. 460, 2019. https://doi.org/10.1016/j.commatsci.2018.12.024.